AN ACCURATE AND EFFICIENT VISCOUS INTERACTION APPROACH FOR ANALYSIS AND DESIGN OF AIRFOILS AND HIGH-LIFT CONFIGURATIONS

A. Verhoff*, T. Michal‡ and T. Cebeci†
McDonnell Douglas Corporation
Saint Louis, Missouri

Abstract

An accurate, comprehensive interactive boundary-layer (IBL) method has been coupled with an analytic-based Euler equation solution method for the analysis and design of airfoils and high-lift configurations. The goal of this development effort is an efficient design process which includes all necessary physics (i.e., compressibility and viscosity). It takes full advantage of the efficiency afforded by an inverse boundary-layer method for predicting viscous effects. The boundary-layer method includes an improved Cebeci-Smith eddy viscosity formulation and computes transition onset using either the e^n-method or Michel's formula. The inviscid-flow method is significantly more efficient than the conventional CFD (Computational Fluid Dynamics) approach for inviscid flow prediction and provides full compressibility effects. It uses a sequence of transformations, mappings and asymptotic methods which places the Euler equations in the form of a boundary value problem amenable to analytic solution using classical mathematical techniques. Furthermore, aerodynamic sensitivity derivatives for design can be evaluated analytically by differentiating and using the same mathematical solution techniques. Results are presented for airfoils and two-element high-lift configurations which demonstrate the potential improvements that can be realized by this approach.

Introduction

There are many CFD methods at the present time which provide accurate numerical predictions for compressible, viscous airfoil flowfields. The analysis cost of these methods in terms of present day computer resources is usually very reasonable. However, when used for high lift prediction, a low free stream Mach number typical of such a condition slows the convergence rate for most methods thereby increasing calculation time, often prohibitively. When used in a design or optimization procedure, a CFD code is often run hundreds of times, especially when many design variables are used. The resulting cost of such a process in terms of computer time can become quite large, even for design points at moderate lift conditions. Extension of the CFD procedure to three dimensions to design a wing, for example, usually requires a large mainframe computer having very large memory. The computer run times can be prohibitive, especially in an advanced design environment. To make the problem tractable, the designer is often forced to limit the number of design variables, thereby compromising the size of the design space.

The first stage in the development of a design process which addresses the difficulties associated with high-lift flowfield prediction noted above is described herein. This involves coupling of an analytic-based Euler method (instead of a panel method) with an accurate IBL method. The resulting method includes all of the required elements for high-lift design calculations, namely, laminar/turbulent viscous interactions, full compressibility effects, and significant efficiency advantages compared to Navier-Stokes CFD methods. Viscous effects are calculated using the efficient IBL method described briefly in the following section and in detail elsewhere.[1] It is well documented that boundary layer methods, when their use is appropriate, are significantly more efficient than a Navier-Stokes CFD method. The inviscid portion of the flowfield is computed using a modification of an analytic-based Euler method.[2][3] Efficiency gains of an order-of-magnitude or more have been demonstrated compared to Euler CFD methods. Because of its underlying analytic foundation, aerodynamic design sensitivities can also be calculated very efficiently, avoiding the expensive CFD approach of differencing numerical solutions in order to estimate sensitivity derivatives.

* MDC Research Fellow
‡ Senior Project Engineer
† MDC Distinguished Fellow

The IBL method has previously been coupled with a panel method and has produced very accurate results for incompressible airfoil flows over a wide range of angle of attack, including stall and post-stall conditions.[4] This combined IBL/panel method has also been applied to multielement airfoils.[5][6][7] Calculations for single and multi-element airfoils along with experiments indicate that compressibility effects can have a significant influence on the accuracy of maximum lift and post-stall flow prediction, and must be included in the calculation method. Compressibility corrections such as Prandtl-Glauert or Karman-Tsien provide some accuracy improvement but in general were found to be inadequate when local flow approaches sonic conditions.[1] Coupling of the IBL method with a full potential or Euler CFD method allows full compressibility and transonic effects to be included in the predictions. However, there is an associated large penalty in efficiency because Euler methods are typically slow to converge at low free stream Mach numbers. Furthermore, field grids must be constructed for the CFD methods which are not required for the panel method implementation.

The analytic Euler method has been introduced to provide compressibility effects in an efficient manner. The method uses an approach for solving the inviscid fluid dynamic equations which is radically different from the conventional CFD approach. A sequence of transformations and mappings is applied to the Euler equations which places them in the form of a boundary value problem amenable to analytic solution using classical mathematical techniques (e.g., integral transforms, Fourier analysis, etc.). Very accurate and highly efficient (by more than two orders of magnitude) asymptotic approximations can be developed based on solution of a simplified linear homogeneous system of equations. Such an approximation has provided the basis for an extremely efficient airfoil design optimization method[8] as compared to the CFD-based approach, which relies on finite differencing of CFD solutions to estimate aerodynamic sensitivities. When local surface velocities approach sonic conditions and compressibility effects are extremely strong, fully accurate solutions can be obtained using asymptotic iterative correction starting from the approximate solution. The approach does not require a computational grid which further enhances its efficiency in comparison to CFD. Furthermore, it is not plagued by the low free stream Mach number restriction which drastically reduces the convergence rate of most CFD Euler and Navier-Stokes methods. The approach has recently been extended and demonstrated for two-element airfoils typical of high-lift systems.[9]

Underlying the analytic Euler formulation is an analytic representation of geometry in terms of orthogonal Chebyshev polynomials.[2] This permits airfoil geometries and displacement surfaces to be described by a minimal number of design variables, which is a necessity for an efficient design optimization method. It is applicable to multielement high-lift configurations. Because the fluid dynamics formulation and geometry representation are analytic-based, design sensitivities can be evaluated very efficiently simply by differentiating and calculating sensitivity derivatives using the same approach used for the fluid dynamic equations.

To couple with the IBL method, the Euler solution method[2][3] must be extended to include wake displacement surfaces. This extension is described below along with the coupling procedure for the IBL method. Results are presented for single and two-element airfoils which validate the accuracy of the coupled procedure.

Interactive Boundary Layer Method

The IBL method used here is an inverse finite-difference method.[1] It employs Veldman's interaction law based on the Hilbert integral formulation and an improved Cebeci-Smith algebraic eddy viscosity formulation that provides much better accuracy for pressure gradient flows than the original model. The improvements in the turbulence model occur in the parameter α and the intermittency expression γ used in the outer eddy viscosity formula. The model is represented by

$$\varepsilon_m = \begin{cases} (0.4y)^2[1-e^{-y/A}]^2\left|\dfrac{\partial u}{\partial y}\right| \\ \\ \alpha u_e \delta^* \gamma \end{cases}$$

In this expression y is the boundary-layer normal coordinate, δ^* is the displacement thickness, u_e is the edge velocity, and A is a damping-length parameter. In the original formulation α was taken as 0.0168; in the improved formulation α is expressed as a function of a Reynolds number defined by the ratio of wall shear to maximum Reynolds shear within the boundary layer. Whereas the previous intermittency expression was valid only for zero pressure gradient flows, the new expression based on Field and Head's correlation[1] is applicable for flows with favorable and adverse pressure gradients, in addition to zero pressure gradient flows.

In the present IBL method, the location of the onset of transition is computed with either the e^n-method or Michel's formula.[1] Calculation of this location is required in order to properly identify the effects of wind tunnel and flight Reynolds number. For example, at wind tunnel Reynolds numbers the individual components of multielement airfoils can experience relatively lower Reynolds numbers than the main airfoil. At chord Reynolds numbers less than 500,000, the components can have large separation bubbles with the onset of transition occurring inside the separation bubble. As a result, the behavior of the flow can be significantly different from the behavior of flow on the airfoil at higher (flight) Reynolds numbers. Thus, the calculation of transition onset must be a part of the computational procedure for the prediction of high-lift configurations.

The calculation procedure begins with the inviscid flow solution obtained for a specified geometry. The inverse boundary-layer method obtains solutions on the upper and lower surfaces starting from the stagnation point. If the onset of transition location is not specified, the laminar flow solutions are used to calculate the transition location by using either Michel's formula or the e^n-method.[1] The viscous flow solutions are then obtained for both the laminar and turbulent flow portions on the airfoil and flap and in the wakes, with calculations taking place separately on the upper and lower surfaces of the bodies and wakes. For a given external velocity distribution, these calculations are repeated until convergence is achieved. Each boundary-layer calculation, starting at the stagnation point and ending at some specified far-field location in the wake is called a sweep. At the completion of the boundary-layer sweeps over the airfoil and flap and in the wakes, the displacement surface, the blowing velocity on the airfoil and flap, and the jump in the normal velocity component in the wakes are known and are used to obtain a new distribution of external velocity from the inviscid method. The boundary-layer calculations are repeated using this updated distribution. As before, the onset of transition location is determined from the laminar flow solutions and the inverse boundary-layer calculations are performed on the upper and lower surfaces of the airfoil and flap and in the wakes by making several sweeps to convergence. This sequence of calculations is repeated for the whole flow field until convergence is achieved.

Inviscid Method

The analytic formulation and details of the solution procedure for the Euler equations are presented in this section. This includes a dependent variable velocity function which contains a nonlinear compressibility correction. The formulation differs from that presented earlier[2][3] so as to provide for the displacement effects of the boundary layers and wakes.

Analytical Formulation

For two-dimensional, steady flow the Euler equations can be written in natural streamline coordinates $(\bar{s},\bar{n})$ as

$$\frac{\partial\theta}{\partial\bar{s}}-\frac{\partial Q}{\partial\bar{n}}=\frac{1}{M^2}\frac{\partial S}{\partial\bar{n}}$$

$$\frac{\partial\theta}{\partial\bar{n}}+\frac{\partial Q}{\partial\bar{s}}=-\frac{2}{\gamma-1}\frac{\partial}{\partial\bar{s}}\ln\left(\frac{a}{a_\infty}\right) \qquad (1)$$

$$a^2+\frac{\gamma-1}{2}q^2=1$$

Velocity magnitude and speed of sound are denoted by q and a, respectively, and Q is the logarithm of velocity normalized to free stream value q_∞. The local Mach number is M and entropy S is defined in terms of pressure p and density ρ as

$$S\equiv\frac{1}{\gamma(\gamma-1)}\ln\left(\frac{p}{\rho^\gamma}\right)=S(\bar{n}) \qquad (2)$$

The flow angle is θ and local distances along and normal to the streamline direction are denoted by $\bar{s}$ and $\bar{n}$, respectively. The streamlines and their normals are defined by the mapping

$$\frac{\partial s}{\partial x}=q\cos\theta \qquad \frac{\partial s}{\partial y}=q\sin\theta$$

$$\frac{\partial n}{\partial x}=-\rho q\sin\theta \qquad \frac{\partial n}{\partial y}=\rho q\cos\theta \qquad (3)$$

The quantities (s,n) are related to velocity potential and stream function, respectively.

The relationships

$$\frac{\partial s}{\partial\bar{s}}=q \qquad \frac{\partial s}{\partial\bar{n}}=0$$

$$\frac{\partial n}{\partial\bar{s}}=0 \qquad \frac{\partial n}{\partial\bar{n}}=\rho q \qquad (4)$$

transform the Euler equations (1) to

$$\frac{\partial\theta}{\partial s}-\frac{\partial Q}{\partial n}=(\rho-1)\frac{\partial Q}{\partial n}+\frac{\rho}{M^2}\frac{\partial S}{\partial n}$$

$$\frac{\partial\theta}{\partial n}+\frac{\partial Q}{\partial s}=\left(1-\frac{1}{\rho}\right)\frac{\partial Q}{\partial s}-\frac{1}{\rho}\frac{2}{\gamma-1}\frac{\partial}{\partial s}\ln\left(\frac{a}{a_\infty}\right) \qquad (5)$$

The homogeneous portion of this system describes incompressible flow. Uniform isentropic upstream flow is assumed and a_∞ refers to the constant value of speed of sound associated with this region. Since the right-hand-side (RHS) of each of Eqs. (5) is relatively small and well-behaved, they are in a form suitable for solution by iteration starting from some initial approximation.

Using the relationship for density,

$$\rho = \left(1 - \frac{\gamma-1}{2} q^2\right)^{\frac{1}{\gamma-1}} e^{-\gamma s} \tag{6a}$$

an asymptotic approximation can be developed, namely,

$$\rho = \left[1 - \frac{1}{2}q^2 + \frac{1}{8}(2-\gamma)q^4 - \frac{1}{48}(2-\gamma)(3-2\gamma)q^6 + \cdots\right] e^{-\gamma s} \tag{6b}$$

By defining a new dependent variable T as

$$T \equiv Q - \frac{1}{4}\left(q^2 - q_\infty^2\right) \tag{7}$$

the Euler equations (5) become

$$\begin{aligned} \frac{\partial \theta}{\partial s} - \frac{\partial T}{\partial n} &= \frac{\partial U}{\partial n} + \frac{\rho}{M^2}\frac{\partial S}{\partial n} - \left(1 - e^{-\gamma s}\right)\left(\frac{\partial T}{\partial n} + \frac{\partial U}{\partial n}\right) \\ \frac{\partial \theta}{\partial n} + \frac{\partial T}{\partial s} &= \frac{\partial V}{\partial s} + \left(1 - e^{\gamma s}\right)\left(\frac{\partial T}{\partial s} - \frac{\partial V}{\partial s}\right) \end{aligned} \tag{8}$$

The quadratic velocity term in the variable T provides a nonlinear compressibility correction.

The functions U and V are functions of velocity only, and have the asymptotic representations

$$U \equiv \frac{1}{32}\left[(2-\gamma)(q^4 - q_\infty^4) - \frac{1}{9}(2-\gamma)(3-2\gamma)(q^6 - q_\infty^6) + \frac{1}{96}(2-\gamma)(3-2\gamma)(4-3\gamma)(q^8 - q_\infty^8) + \cdots\right] \tag{9a}$$

$$V \equiv \frac{1}{32}\left[3\gamma(q^4 - q_\infty^4) + \frac{5}{9}\gamma(2\gamma-1)(q^6 - q_\infty^6) + \frac{7}{96}\gamma(2\gamma-1)(3\gamma-2)(q^8 - q_\infty^8) + \cdots\right] \tag{9b}$$

The system (8) can be viewed as linear, non-homogeneous partial differential equations assuming that the RHS terms are known quantities. In an asymptotic corrective iteration process, these terms (if they are relatively small) can be approximated using previous iteration results. Solution of the homogeneous left-hand-side (LHS) portion provides an initial starting approximation. Upon convergence the process yields the solution to the Euler equations (1).

Initial Inviscid Approximation

An inviscid solution is required to initiate the interactive boundary layer calculation. The initialization is described in this section. It consists of solution procedures for both the homogeneous and non-homogeneous portions of the system (8). The homogeneous portion of the system (8) represents Cauchy-Riemann conditions and can be solved by conformal mapping and other classical mathematical techniques. Only the isentropic terms in the non-homogenous portion are considered here in this initial stage of development. The procedure for including rotational (entropy) effects is described elsewhere.[10]

Homogeneous Solution (Single Element) - A single element airfoil is represented by a slit in the (s,n) plane which is assumed to lie along a portion of the $n = 0$ axis. The mapping from the physical (x,y) plane is defined by the transformations (3) and (4). For inviscid flows producing lift, the upper and lower segments of the slit have unequal length as shown in Figure 1.

The mapping function

$$\tau = K[\cos(w + \delta) - w\sin\delta] + C \qquad \tau \equiv s + in \qquad w \equiv u + iv \tag{10}$$

maps the slit conformally to a semi-infinite strip region defined by $|u| \leq \pi$, $v \geq 0$. The mapping is illustrated in Figure 2. Previously[2][3] an approximate polar mapping was used which did not fully remove the wake discontinuity in the mapped plane (i.e., periodicity error). The associated error was noticeable only downstream along the wake line and only at higher angles of attack. Since the goal of the present method is high-lift analysis, the precise mapping (10) is used. The mapping constants C and K are related to the slit length and the airfoil circulation, which are determined by the airfoil geometry, surface velocity, and lift. The parameter δ is related to the stagnation point location. The solution is periodic in the w-plane.

The surface flow angle boundary conditions, denoted by θ_b, are transferred to the base of the strip by the mapping (10). These Dirichlet conditions are shown schematically in Figure 3 as a function of u for $v=0$. At the stagnation point image (denoted by u_o), there is a discontinuity in θ_b of magnitude π.

The distribution θ_b can be decomposed into several parts, namely,

$$\theta_b = \frac{1}{2}(\varepsilon_u + \varepsilon_l) - \alpha + \frac{1}{2\pi}(\varepsilon_u - \varepsilon_l)u + \frac{1}{4\pi}(\varepsilon'_u - \varepsilon'_l)(u^2 - \pi^2) + \pi U(u_o) + \phi_b \tag{11}$$

The angle of attack is α and

$$\varepsilon_l = \theta_b\big|_{u=-\pi} \qquad \varepsilon_u = -\pi + \theta_b\big|_{u=\pi}$$
$$\varepsilon'_l = \frac{d\theta_b}{du}\bigg|_{u=-\pi} \qquad \varepsilon'_u = \frac{d\theta_b}{du}\bigg|_{u=\pi} \tag{12}$$

The function $U(u_o)$ represents a unit step function located at u_o. The remaining function ϕ_b is smooth, vanishes at $u = \pm\pi$, and has continuous slope at $u = \pm\pi$. With this formulation, the flow angle at infinity θ_∞ can be set to zero as a boundary condition.

Each of the components of θ_b can be represented accurately by means of Fourier series. These representations are

$$(\varepsilon_u - \varepsilon_l)\frac{u}{2\pi} = -\frac{1}{\pi}(\varepsilon_u - \varepsilon_l)\sum_{k=1}^{\infty}\frac{(-1)^k}{k}\sin ku \tag{13}$$

$$\frac{1}{4\pi}(\varepsilon'_u - \varepsilon'_l)(u^2 - \pi^2) = \frac{1}{\pi}(\varepsilon'_u - \varepsilon'_l)\left[-\frac{\pi^2}{6} + \sum_{k=1}^{\infty}\frac{(-1)^k}{k^2}\cos ku\right] \tag{14}$$

$$\pi U(u_o) = \frac{1}{2}(\pi - u_o) - \sum_{k=1}^{\infty}\frac{\sin ku_o}{k}\cos ku + \sum_{k=1}^{\infty}\frac{1}{k}\left[\cos ku_o - (-1)^k\right]\sin ku \tag{15}$$

$$\phi_b = A_o + \sum_{k=1}^{\infty} A_k \cos ku + \sum_{k=1}^{\infty} B_k \sin ku \tag{16}$$

Because of its properties, ϕ_b can be represented to arbitrary accuracy using a finite number of modes (A_k, B_k).

The solution of the homogeneous subset of the system (8) is

$$\theta_h = \sum_{k=1}^{\infty} e^{-kv}\left[C_k \cos ku + D_k \sin ku\right] \tag{17}$$

$$T_h = \sum_{k=1}^{\infty} e^{-kv}\left[C_k \sin ku - D_k \cos ku\right] \tag{18}$$

Application of the boundary conditions (at $v=0$) determines the Fourier coefficients as

$$C_k = A_k - \frac{\sin ku_o}{k} + \frac{1}{\pi}(\varepsilon'_u - \varepsilon'_l)\frac{(-1)^k}{k^2}$$
$$D_k = B_k + \frac{\cos ku_o}{k} - \frac{(-1)^k}{k}\left(1 + \frac{\varepsilon_u - \varepsilon_l}{\pi}\right) \tag{19}$$

For $k=0$ the Fourier mode must vanish which requires

$$u_o - \pi + 2\alpha - 2A_o - \varepsilon_u - \varepsilon_l + \frac{\pi}{3}(\varepsilon'_u - \varepsilon'_l) = 0 \tag{20}$$

This relationship enforces the θ boundary condition at infinity and determines the stagnation point image location u_o.

Some of the components (i.e., summations) of the Fourier series (18) representing T on the boundary can be replaced by their equivalent analytic functions. This provides a large increase in computational efficiency. The boundary (airfoil surface) distribution of T_h then simplifies to

$$T_b = \sum_{k=1}^{\infty}\left[A_k \sin ku - B_k \cos ku\right] - \frac{1}{2}\left(1 + \frac{\varepsilon_u - \varepsilon_l}{\pi}\right)\ln\left[2(\cos u + 1)\right] + \frac{1}{2}\ln\left[2\left|\cos(u - u_o) - 1\right|\right] - \frac{1}{\pi}(\varepsilon'_u - \varepsilon'_l)\left[\frac{5}{4}\sin u - \sin u \ln\left(2\cos\frac{u}{2}\right)\right] + \sum_{k=2}^{\infty}\left[\frac{(-1)^k}{k^2(k^2-1)}\sin ku\right] \tag{21}$$

The first summation in this expression represents a smooth periodic function derived from ϕ_b. The last summation is the result of applying a convergence acceleration transformation. Both summations are rapidly convergent. For evaluation of flow field quantities at off-body points, similar simplifications also exit. Specifically,

$$\begin{aligned} T_h = &\sum_{k=1}^{\infty} e^{-kv}\left[A_k \sin ku - B_k \cos ku\right] \\ &+\frac{\varepsilon'_u - \varepsilon'_l}{\pi}\sum_{k=1}^{\infty} e^{-kv}\frac{(-1)^k}{k^2}\sin ku \\ &+\frac{1}{2}\log\left[1-2e^{-v}\cos(u-u_o)+e^{-2v}\right] \\ &-\frac{1}{2}\left(1+\frac{\varepsilon_u-\varepsilon_l}{\pi}\right)\log\left[1+2e^{-v}\cos u+e^{-2v}\right] \end{aligned} \tag{22}$$

$$\begin{aligned} \theta_h = &\sum_{k=1}^{\infty} e^{-kv}\left[A_k \cos ku + B_k \sin ku\right] \\ &+\frac{\varepsilon'_u - \varepsilon'_l}{\pi}\sum_{k=1}^{\infty} e^{-kv}\frac{(-1)^k}{k^2}\cos ku \\ &+\tan^{-1}\left[\frac{e^{-v}\sin(u-u_o)}{1-e^{-v}\cos(u-u_o)}\right] \\ &+\left(1+\frac{\varepsilon_u-\varepsilon_l}{\pi}\right)\tan^{-1}\left[\frac{e^{-v}\sin u}{1+e^{-v}\cos u}\right] \end{aligned} \tag{23}$$

These relations provide information for initial evaluation of the functions U and V which appear in Eqs. (8) and are defined by Eqs. (9). An initial approximation of these RHS terms is needed to start the corrective iteration process. The transformation (10) provides the mapping of the (u,v) coordinates back to the (s,n) space.

Homogenous Solution (Two Elements) - A two-element configuration is represented by two slits in the (s,n) plane. The main airfoil element is assumed to lie along a portion of the n=0 axis. The flap element is displaced an amount $(\Delta s, \Delta n)$ as shown in Figure 4.

The transformation

$$\begin{aligned} \tau = -\frac{\Delta n}{\pi}\Big[\ &w+\frac{1}{2}b e^{2w}-(1+b)e^{w} \\ &+\frac{1}{2}b+1\ \Big] \end{aligned} \tag{24}$$

$$\tau = s + in \qquad w = u + iv$$

where b satisfies

$$b-\frac{1}{b}-2\ln|b|+2\pi\frac{\Delta s}{\Delta n}=0 \tag{25}$$

maps the two slits onto the boundaries of an infinite strip of width π. This mapping is illustrated in Figure 5 and is a combination of a Schwarz-Christoffel transformation and an exponential mapping. The main airfoil element lies on the lower boundary between w_1 and w_2 with its stagnation point at w = 0. The flap element lies on the upper boundary between w_3 and w_4 with its stagnation point at $w = -\ln|b| + i\pi$.

The surface flow angle boundary conditions for the airfoil and flap are transferred to the boundaries of the strip by the mapping (24). These Dirichlet conditions are denoted by θ_b^a and θ_b^f, respectively. At the stagnation points there are discontinuities of magnitude π, with lesser discontinuities at the trailing edge images.

The solution of the homogeneous subset of the system (8) can be obtained using integral transforms. The solution for T_h is

$$\begin{aligned} T_n = &\frac{1}{2\pi}\int_{-\infty}^{\infty}\frac{\sinh(\sigma-u)\theta_b^f(\sigma)}{\cosh(\sigma-u)+\cos v}\,d\sigma - \\ &\frac{1}{2\pi}\int_{-\infty}^{\infty}\frac{\sinh(\sigma-u)\theta_b^a(\sigma)}{\cosh(\sigma-u)-\cos v}\,d\sigma \end{aligned} \tag{26}$$

The corresponding solution for θ_n is

$$\begin{aligned} \theta_n = &\frac{1}{2\pi}\int_{-\infty}^{\infty}\frac{\sin v\ \theta_b^f(\sigma)}{\cosh(\sigma-u)+\cos v}\,d\sigma + \\ &\frac{1}{2\pi}\int_{-\infty}^{\infty}\frac{\sin v\ \theta_b^a(\sigma)}{\cosh(\sigma-u)-\cos v}\,d\sigma \end{aligned} \tag{27}$$

For the initial inviscid solution, approximate values of θ_b^a and θ_b^f can be prescribed for the wake portions of the two boundaries. These values can be corrected subsequentially during the viscous interaction phase of the solution. The stagnation point locations in physical space are determined such that the condition

$$\int_{-\infty}^{\infty}\left(\ \theta_b^a - \theta_b^f\ \right)d\sigma = 0 \tag{28}$$

is satisfied and $T_n = 0$ in the far field. These solutions provide the initial information to start the

viscous interaction process and for initial evaluation of the functions U and V which appear in Eqs. (8).

Non-Homogeneous Solution - An expedient strategy for obtaining solutions of the non-homogeneous system (8) is to construct a Green's function formulation. Green's function construction can be accomplished in a straightforward manner using classical techniques. The solutions of the homogeneous system described above satisfy the exact surface flow angle boundary conditions. It is therefore advantageous that the non-homogenous solution satisfy $\theta = 0$ along the element surfaces.

The Green's function is constructed for the upper half-plane in order to be applicable to both the inviscid and the coupled viscous analyses. It also provides for single and multielement configurations. The mapping required to transform the flowfield to the upper half-plane for a single airfoil is

$$\tau = \zeta^2 \qquad \zeta \equiv \xi + i\eta \tag{29}$$

The airfoil image in the (s,n) plane is unwrapped and lies along the real axis. The isentropic Euler equations (8) become

$$\frac{\partial\theta}{\partial\xi} - \frac{\partial T}{\partial\eta} = R_1 \qquad \frac{\partial\theta}{\partial\eta} + \frac{\partial T}{\partial\xi} = R_2 \tag{30}$$

where

$$R_1 \equiv \frac{1}{\xi^2+\eta^2}\left[\xi^2\frac{\partial U}{\partial\eta} - \eta^2\frac{\partial V}{\partial\eta} + \xi\eta\frac{\partial}{\partial\xi}(U+V)\right]$$

$$R_2 \equiv \frac{1}{\xi^2+\eta^2}\left[\xi^2\frac{\partial V}{\partial\xi} - \eta^2\frac{\partial U}{\partial\xi} - \xi\eta\frac{\partial}{\partial\eta}(U+V)\right] \tag{31}$$

For a multielement configuration the mapping required (Schwarz-Christoffel) is

$$\tau = \frac{-\Delta n}{\pi}\left[\ \log\zeta + \frac{1}{2}b\zeta^2 - (1+b)\zeta + \frac{1}{2}b + 1\ \right] \tag{32}$$

Both elements are unwrapped and lie along the real axis. The corresponding RHS terms are similar to those defined by Eqs. (31), but with the transformation metrics of the mapping (32).

The Green's function for the upper half-plane can be constructed using integral transforms. The particular solution for the non-homogeneous system (30) may then be expressed as

$$T_p = \frac{1}{2\pi}\int_{-\infty}^{\infty}\int_{o}^{\infty}\frac{(\xi-\sigma)R_2 - (\eta-\mu)R_1}{(\xi-\sigma)^2+(\eta-\mu)^2}\,d\mu d\sigma + \frac{1}{2\pi}\int_{-\infty}^{\infty}\int_{o}^{\infty}\frac{(\xi-\sigma)R_2 + (\eta+\mu)R_1}{(\xi-\sigma)^2+(\eta+\mu)^2}\,d\mu d\sigma \tag{33}$$

$$\theta_p = \frac{1}{2\pi}\int_{-\infty}^{\infty}\int_{o}^{\infty}\frac{(\xi-\sigma)R_1 + (\eta-\mu)R_2}{(\xi-\sigma)^2+(\eta-\mu)^2}\,d\mu d\sigma - \frac{1}{2\pi}\int_{-\infty}^{\infty}\int_{o}^{\infty}\frac{(\xi-\sigma)R_1 - (\eta+\mu)R_2}{(\xi-\sigma)^2+(\eta+\mu)^2}\,d\mu d\sigma \tag{34}$$

Note that θ_p vanishes on the real axis (i.e., η=0).

The double quadrature required to evaluate T_p and θ_p can be carried out to any required accuracy by a variety of methods. A bi-linear approximation for the functions R_1 and R_2 over discrete quadrilateral cells allows local analytic quadrature, and removes the Green's function singularities. This approach has been used with good success.

Each non-homogeneous solution provides an improved approximation of the velocity function T and the RHS terms R_1 and R_2. Iteration of the process yields an asymptotic solution of the Euler equations to any degree of accuracy. From the converged solution the pressure distribution on the airfoil surface and wake can be determined for input to the boundary-layer method.

Viscous Interaction

The initial boundary-layer solution defines an approximate displacement surface around the airfoil elements and wakes which must be taken into account in subsequent inviscid solution iterations. The initial inviscid solution defines a first approximation to the wake dividing streamline but does not include wake displacement effects. Different procedures must be used for single and multielement airfoils to include wake displacement effects on the inviscid flowfield. These procedures are described in this section.

Single Element Configuration - The airfoil and wake displacement surfaces are mapped to a semi-infinite slit in the (s,n) plane. This slit can be mapped to the real axis by the transformation (29). The flowfield is mapped to the upper half-plane. Values of flow angle along the displacement surface, denoted by θ_d, are provided by the boundary-layer solution. These Dirichlet boundary values are mapped to the

real axis of the upper half–plane. The solution of both the homogeneous and non-homogeneous portions of the system (30) is carried out in the upper half-plane. A Green's function analysis provides the solution of the homogeneous portion of the system (30) as

$$\theta_h = \frac{1}{\pi}\int_{-\infty}^{\infty} \frac{\eta\theta_d}{(\xi-\sigma)^2+\eta^2} d\sigma$$

$$T_h = \frac{1}{\pi}\int_{-\infty}^{\infty} \frac{(\xi-\sigma)\theta_d}{(\xi-\sigma)^2+\eta^2} d\sigma \qquad (35)$$

Quadrature along the real axis for a given value of η is used to evaluate T_h and θ_h. The solution for the non-homogeneous system is again provided by the solution (33-34). The homogeneous solution (35) provides initial values for evaluating the quantities R_1 and R_2. Corrective iteration produces a converged inviscid solution to the Euler equations (30) for the flowfield outside the displacement surface. Pressure distributions from this solution provide the input for the boundary-layer method.

As the viscous/inviscid solution iterations are carried out, the position of the wake dividing streamline must be adjusted to account for the interactions, especially at higher angles of attack. The adjustment is dictated by the jump in normal velocity across the dividing streamline which is provided by the boundary-layer solution. Procedures for correcting the wake position are outlined in References 1 and 11. The wake correction has not been introduced at this point in the development.

Two-Element Configurations - The same solution procedure used for the initial inviscid approximation for two elements is used to include displacement effects by changing the surface boundary conditions to flow angle values along the displacement surfaces. These values are provided by the viscous solution. Homogenous solutions are provided by Eqs. (26-27) and non-homogenous solutions by Eqs. (33-34). Pressure distributions from these solutions again provide the input for the boundary layer method.

Results

Results are presented in this section which validate the accuracy of this new viscous/inviscid interaction method. Comparisons are made with a panel method/IBL procedure and also with test data. The improved accuracy in predicting compressibility effects are also demonstrated. Preliminary efficiency information is provided.

Single Element Configurations

The incompressible pressure distribution for a NACA 0012 airfoil at an angle of attack of 6 degrees calculated using the new Euler/IBL method is shown in Figure 6. The prediction provided by the panel method/IBL procedure[4] is also shown for comparison. The results are nearly identical except near the trailing edge. This is possibly due to the different treatment of the trailing edge region. The panel method imposes a Kutta condition of equal velocity on the upper and lower displacement surfaces at the trailing edge location. The Euler method uses the displacement surface flow angle as boundary values to compute the outer inviscid flowfield without imposing any relationship on these values across the viscous layer. The skin friction distributions are compared in Figure 7. There is good agreement with a slight difference near the trailing edge. The onset of transition occurs at approximately 5 percent chord on the upper surface and 80 percent chord on the lower surface.

Lift and drag results for the NACA 0012 airfoil compared with test data[12] are shown in Figures 8 and 9. The flow was incompressible and the Reynolds number was 9 million. Correlation with test data is good. The calculations were limited to angles of attack less than 12 degrees because the new method does not yet have a wake correction capability. The wake dividing streamline position was held fixed at the location determined by the initial inviscid solution. Separation starts to occur at approximately 8 degrees which can have a large effect on wake position. Correction of the wake position becomes important in this range because of the increased curvature just downstream of the trailing edge. This possibly accounts for the slight departure from the test data at the higher angles of attack.

The computational cost (i.e, computer time) of these calculations is approximately the same for both methods. A Navier-Stokes CFD calculation is typically more than an order of magnitude more expensive.

The primary reason for replacing the panel method with the Euler formulation in a viscous interaction method is to provide the capability of including full compressibility affects. The benefits are shown in Figure 10 for a NACA 0012 airfoil at a free stream Mach number of 0.63 and an angle of attack of 2 degrees. At this condition the peak Mach number on the airfoil surface is 0.98. There is considerable difference between the analytic Euler solution and the panel method result which uses a Prandtl-Glauert compressibility correction. The incompressible solution is shown for reference. Also shown is an Euler solution using the FLO67-2D CFD code[13]. The analytic Euler and CFD solutions are

nearly identical and predict lift coefficients differing by approximately one percent.

Two-Element Configurations

The Euler/IBL method has been applied to a NACA airfoil/flap configuration[14] and results are shown in Figures 11 and 12. The main element was a NACA 4412 section and the flap element was a NACA 4415 section. The flap element was at ten degrees incidence with respect to the main element. Figure 11 compares the experimental pressure distribution (incompressible conditions) at a Reynolds number of 1.3 million and an angle of attack of 2.2 degrees with those predicted by the panel method/IBL procedure and the Euler/ IBL analytical method. Predicted skin friction results are shown in Figure 12. Agreement is generally good. The Euler/IBL predictions on the flap element are very sensitive to the main element wake location which accounts for the small discrepancy on the upper surface of the flap element. Correction of the wake position due to viscous interactions in this vicinity is needed. There is some difference in the predicted transition locations on the main element evident in Figure 12. There is also some difference in the separation location on the flap element.

Summary

An accurate, efficient IBL method has been coupled with an analytic-based Euler solution method and the accuracy of the new procedure has been demonstrated for single and multielement airfoils. Lift and drag predictions compare well with test data. More accurate prediction of compressibility effects compared to the typical panel method implementation is the major improvement. The new procedure also avoids the difficulties of enforcing a Kutta condition associated with the panel method implementation. Efficiency of the new method is comparable to the IBL/panel method procedure and more than an order of magnitude greater than a CFD Navier-Stokes method. A correction method for wake position changes due to viscous interactions remains to be implemented.

References

1. Cebeci, T., An Engineering Approach to the Calculation of Aerodynamic Flows, to be published, 1996.

2. Verhoff, A., Stookesberry, D., and Cain, A. B., "An Efficient Approach to Optimal Aerodynamic Design Part 1: Analytic Geometry and Aerodynamic Sensitivities," AIAA Paper No. 93-0099, Jan. 1993.

3. Verhoff, A., and Stookesberry, D., "Solution of the Euler Equations for Airfoils Using Asymptotic Methods," AIAA Paper No. 93-2931, July 1993.

4. Cebeci, T., Hefazi, H., Roknaldin, F., and Carr, L. W., "Predicting Stall and Post-Stall Behavior of Airfoils at Low Mach Numbers," AIAA Journal, Vol. 33, No. 4, April 1995, pp. 595-602.

5. Cebeci, T., "Calculation of Multielement Airfoils and Wings at High Lift," AGARD Conference Proceedings 515 on High-Lift Aerodynamics, Paper No. 24, Banff, Alberta, Canada, Oct. 1992.

6. Cebeci, T., Besnard, E., and Messie, S., "A Stability/Transition-Interactive-Boundary-Layer Approach to Multielement Wings at High Lift," AIAA Paper No. 94-0292, Jan. 1994.

7. Cebeci, T., Besnard, E., and Chen, H., "Calculation of Multielement Airfoil Flows, Including Flap Wells," AIAA Paper No. 96-0056, Jan. 1996.

8. Stookesberry, D., Verhoff, A., and Cain, A. B., "An Efficient Approach to Optimal Aerodynamic Design Part 2: Implementation and Evaluation," AIAA Paper No. 93-0100, Jan. 1993.

9. Verhoff, A., Michal, T., and Stookesberry, D., "Solution of the Euler Equations for Two-Element Airfoils Using Asymptotic Methods," AIAA Paper No. 94-0082, Jan. 1994.

10. Verhoff, A., Stookesberry, D., and Michal T., "Transonic Euler Solutions for Airfoils Using Asymptotic Iterative Corrections: Analysis," AIAA Paper No. 94-2198, June 1994.

11. Lock, R. C., and Williams, B. R., "Viscous-Inviscid Interactions in External Aerodynamics," Progress in Aerospace Science, Vol. 24, No. 2, 1987, pp. 51-171.

12. Abbot, I. H., and Von Doenhoff, A. E., Theory of Wing Sections, Dover, 1959.

13. Jameson, A., "A Vertex Based Multigrid Algorithm for Three-Dimensional Flow Calculations," ASME AMD, Vol. 78, American Society of Mechanical Engineers, New York, Dec. 1986, pp. 45-73.

14. Olson, L. E., and Orloff, K. L., "On the Structure of Turbulent Wakes and Merging Shear Layers of Multi-Element Airfoils," AIAA Paper No. 81-1238, June 1981.

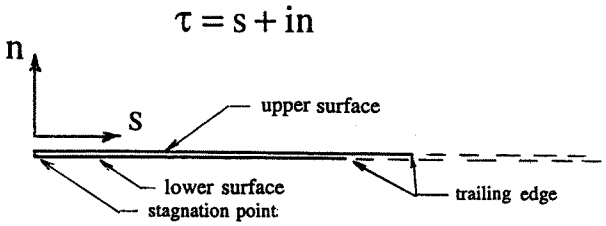

Fig. 1 Airfoil Image In Streamline Coordinate Plane

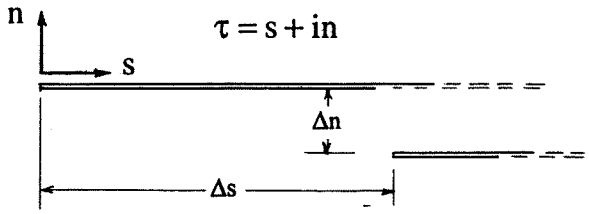

Fig. 4 Two-Element Airfoil Image in Streamline Coordinate Plane.

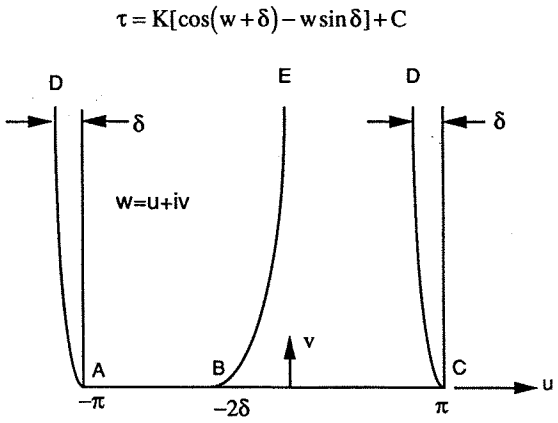

Fig. 2 Mapping to Semi-Infinite Strip

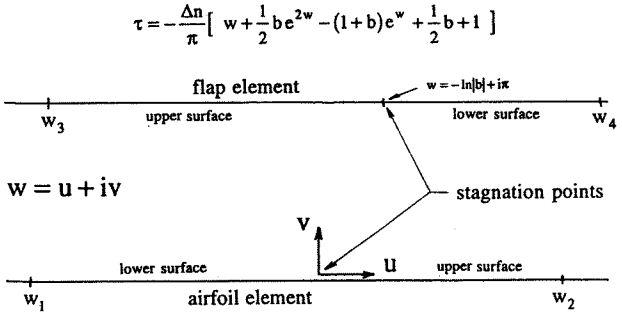

Fig. 5 Mapping to Infinite Strip.

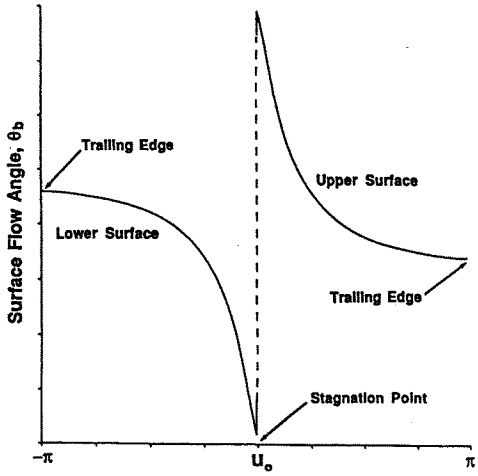

Fig. 3 Airfoil Surface Flow Angle Distribution

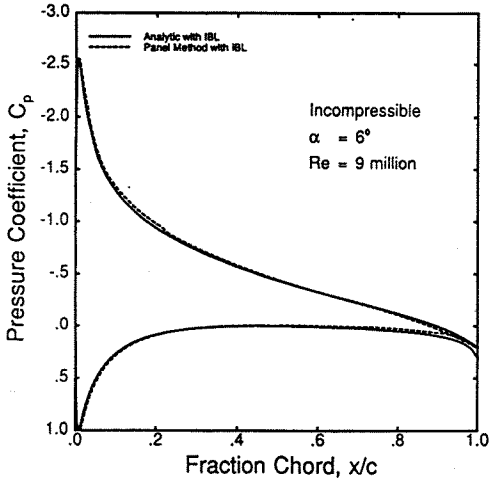

Fig. 6 Incompressible Pressure Predictions for NACA 0012 Airfoil

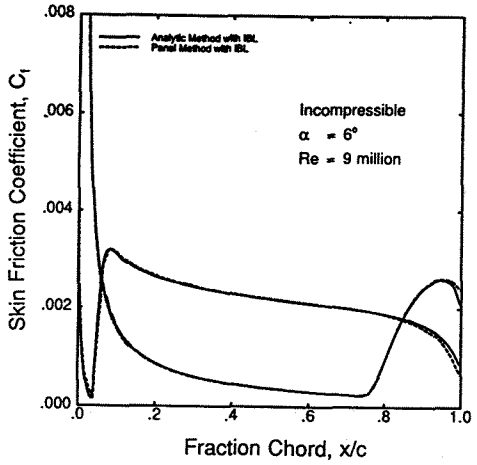

Fig. 7 Incompressible Skin Friction Predictions for NACA 0012 Airfoil

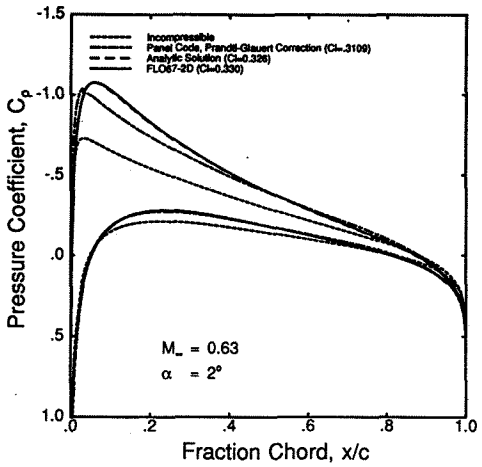

Fig. 10 Inviscid Compressible Pressure Predictions for NACA 0012 Airfoil

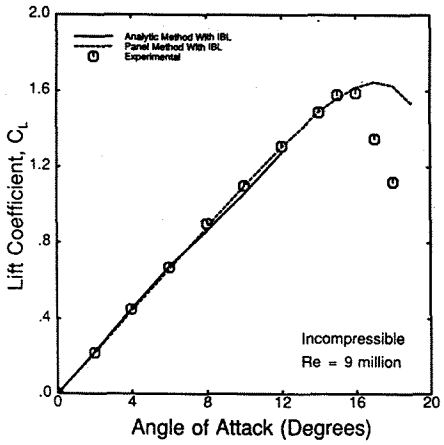

Fig. 8 Lift Curve Predictions Compared With Test Data for NACA 0012 Airfoil

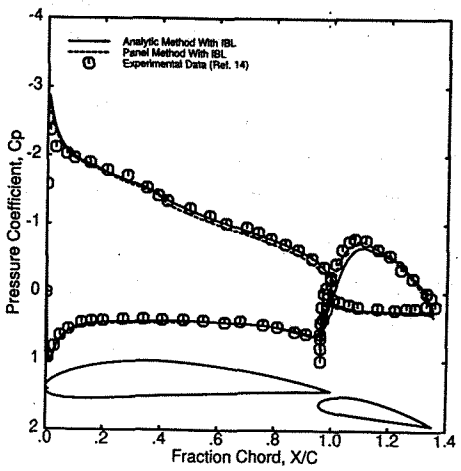

Fig. 11 Pressure Predictions Compared With Test Data for Two-Element Airfoil.

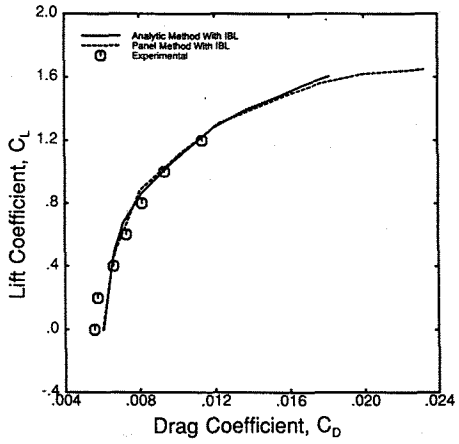

Fig. 9 Drag Polar Predictions Compared With Test Data for NACA 0012 Airfoil

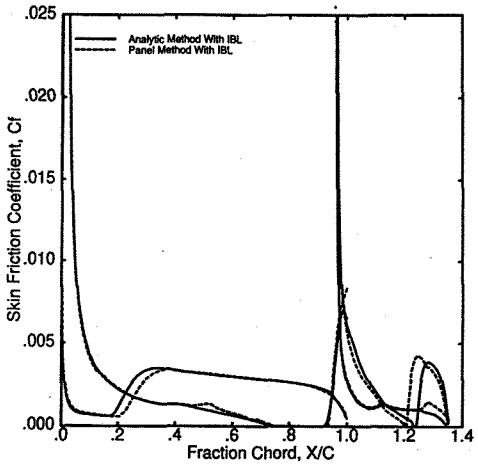

Fig. 12 Skin Friction Predictions for Two-Element Airfoil.